Available online at www.sciencedirect.com
SCIENCE DIRECT
Bioorganic & Medicinal Chemistry 14 (2006) 2197–2208
Bioorganic & Medicinal Chemistry

Macrocyclic inhibitors of the malarial aspartic proteases plasmepsin I, II, and IV

Karolina Ersmark,[a] Martin Nervall,[b] Hugo Gutiérrez-de-Terán,[b] Elizabeth Hamelink,[c] Linda K. Janka,[d] Jose C. Clemente,[d] Ben M. Dunn,[d] Adolf Gogoll,[e] Bertil Samuelsson,[c] Johan Åqvist[b] and Anders Hallberg[a,*]

[a]*Department of Medicinal Chemistry, Uppsala University, BMC, PO Box 574, SE-751 23 Uppsala, Sweden*
[b]*Department of Cell and Molecular Biology, Uppsala University, BMC, PO Box 596, SE-751 24 Uppsala, Sweden*
[c]*Medivir AB, Lunastigen 7, SE-141 44 Huddinge, Sweden*
[d]*Department of Biochemistry and Molecular Biology, University of Florida College of Medicine, BMC, PO Box 100245 Gainesville, FL 32610-0245, USA*
[e]*Department of Organic Chemistry, Uppsala University, BMC, PO Box 599, SE-751 24 Uppsala, Sweden*

Received 1 September 2005; accepted 2 November 2005
Available online 22 November 2005

Abstract—The first macrocyclic inhibitor of the *Plasmodium falciparum* aspartic proteases plasmepsin I, II, and IV with considerable selectivity over the human aspartic protease cathepsin D has been identified. A series of macrocyclic compounds were designed and synthesized. Cyclizations were accomplished using ring-closing metathesis with the second generation Grubbs catalyst. These compounds contain either a 13-membered or a 16-membered macrocycle and incorporate a 1,2-dihydroxyethylene as transition state mimicking unit. The binding mode of this new class of compounds was predicted with automated docking and molecular dynamics simulations, with an estimation of the binding affinities through the linear interaction energy (LIE) method.

1. Introduction

Malaria has in recent years re-emerged as one of the most serious infectious diseases in the world. This is primarily due to the rapid spread of parasite drug resistance, in particular among the most lethal species affecting humans, *Plasmodium falciparum*.[1] Each year approximately 300–500 million clinical cases are reported and 1–3 million people, mostly children in Africa, die as a result of the disease.[2] Several attempts are being made to develop new antimalarial drugs with novel mechanisms of action.[3] The malarial aspartic proteases, termed plasmepsins, have been identified as one class of suitable targets.[4] Proof of concept that these enzymes are essential for parasite survival has been provided both from cell culture and animal models.[5,6] The precise role of each of the ten plasmepsins found in the *P. falciparum* genome is not yet fully understood.[4] However, four of them, plasmepsin (Plm) I, II, IV, and the closely related histo-aspartic protease (HAP), have been demonstrated to be active in the food vacuolar hemoglobin catabolism.[7] Of these, the first characterized, Plm I and II, have so far been most extensively investigated as targets for inhibitor design.[6,8] Recent studies employing parasite knockout clones suggest that efficient antiparasitic agents should target not only one but several of the food vacuole plasmepsins.[9,10]

We have previously identified linear Plm I and II inhibitors, which incorporate a mannitol-derived 1,2-dihydroxyethylene unit, as a common transition state isostere.[11–13] In this series of compounds, a number of nanomolar activity inhibitors with a considerable discrimination versus the most homologous human aspartic protease cathepsin D (Cat D) as a characteristic feature were discovered.

Keywords: Malaria; Plasmepsin; Protease inhibitors and molecular dynamics.
* Corresponding author. Tel.: +46 18 471 42 84; fax: +46 18 471 44 74; e-mail: anders.hallberg@orgfarm.uu.se

0968-0896/$ - see front matter © 2005 Elsevier Ltd. All rights reserved.
doi:10.1016/j.bmc.2005.11.003

Aspartic proteases usually bind substrates/inhibitors adopting an extended β-strand conformation.[14] By enabling preorganization of the inhibitor in a bioactive conformation, a higher affinity should be achieved due to a reduced loss of entropy upon binding.[14] Macrocyclization has previously proven to be an effective constraining device in aspartic protease inhibitors.[15–19] Additionally, constrained compounds with amide bonds demonstrate a higher resistance to proteolytic cleavage, and macrocyclic compounds often exhibit improved cell permeability compared to their acyclic counterparts.[16,20] To the best of our knowledge, only two plasmepsin inhibitors with a macrocyclic structural element have been reported.[19,21] A statine-based inhibitor containing a bridge between the P1 and P3 side chains that forms a 15-membered macrocycle exhibited a high potency against Plm II (**1**, Fig. 1). On the contrary, an inhibitor with a P2-P3′ 20-membered macrocycle originating from the same type of statin scaffold lost potency for Plm II (**2**, Fig. 1).[19] However, more recently the latter inhibitor was shown to inhibit Plm IV efficiently.[21] Unfortunately, none of these macrocyclic inhibitors was selective over the human Cat D.

We felt encouraged to investigate whether non-prime side or prime/non-prime side macrocyclizations of the previously reported prototype C_2-symmetric inhibitors encompassing amino indanol structures in both the P2 and P2′ positions would deliver, first of all, inhibitors of Plm I, II, or IV, and secondly, inhibitors of these proteases that were devoid of Cat D affinity. Compounds **3** and **4** in Table 1 were used as starting structures and ring-closing metathesis (RCM) rather than amide bond formation was employed to avoid incorporation of a new hydrogen bond-accepting/donating amide in the macrocycle. Two ring sizes were explored: a 13-membered ring connecting the P1 and P2 positions or the P1′ and P2′ positions, depending on the binding mode to the plasmepsin, and a 16-membered ring with a P1–P2′/P2–P1′ connection. The smaller 13-membered rings were designed to be accommodated in the unobstructed S1–S3 cleft, while the 16-membered rings were included to address the previous observation that a large cycle spanning over both the prime and non-prime sides is well accommodated in Plm IV but is far less potent against Plm II.[19,21] The binding features of the new macrocyclic inhibitors were investigated by molecular modeling.

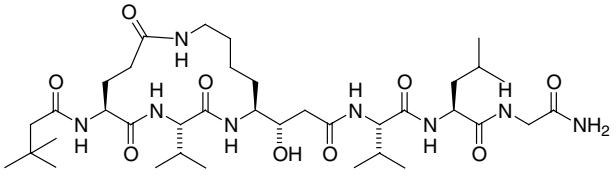

1. K_i Plm II, 0.2 nM; K_i Cat D, 0.26 nM.[19]

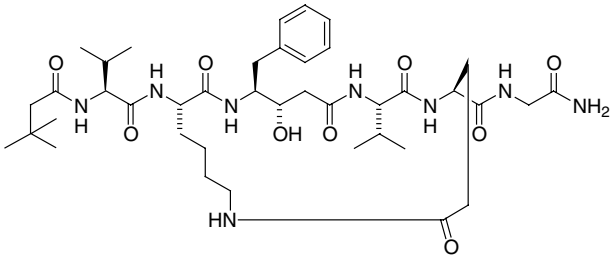

2. K_i Plm II, 1500 nM;[19] K_i Plm IV, 0.52 nM;[21] K_i Cat D, 1.4 nM.[19]

Figure 1. Macrocyclic plasmepsin inhibitors previously reported in the literature.

Herein we report that RCM with the second generation Grubbs catalyst delivers the first macrocyclic plasmepsin inhibitors with significant selectivity over Cat D.

2. Results

2.1. Chemistry

Scheme 1 outlines the synthetic route to the unsaturated and saturated macrocyclic target compounds **5**–**8**. The intermediate compounds **12** and **13** were synthesized essentially following a previously reported strategy.[22] Alkylation of L-mannaro-1,4:3,6-di-γ-lactone was accomplished using simultaneous addition of 1.5 equiv benzyl trichloroacetimidate and 1.5 equiv allyl trichloroacetimidate yielding approximately a 1:1:1 mixture of the diallylated[11] and the dibenzylated[23] bislactones together with the unsymmetrically allylated and benzylated bislactone, **9**. Mono-opening of bislactone **9** was accomplished with (1*S*,2*R*)-1-amino-2-indanol using 2-hydroxypyridine as catalyst to give the mono-lactones **10** and **11**, which could not be completely separated. No obvious preference in the opening of the two lactones of **9** was observed. Approximately a 1:1 ratio of compounds **10** and **11** was formed as deduced from LC–MS. Finally, the second lactone ring was opened using excess octenamine (**14**) to afford a mixture of the two intermediate compounds **12** and **13** in 73% yield. As a consequence of **12** and **13** being inseparable on the LC systems available, these isomers were used as a mixture in the subsequent RCM. A second generation Grubbs catalyst[24] was employed in the RCM, which was conducted in 1,2-dichloroethane at reflux. The four resulting macrocycle diastereomers, i.e., the *E* and *Z* isomers of **5** and **7**, were separated by LC. ^{1}H NMR was used to determine the *E*:*Z* ratios. To identify the 13-membered macrocycle (**5**) and the 16-membered macrocycle (**7**), C–H connectivity information from HMBC NMR experiments was used. Thus, starting with H-1 (Scheme 1), identified by its connectivity to the hydroxyindan moiety, H-3 can be located via C–H long-range couplings. Proton H-1 (denoted in **5** and **7**, Scheme 1) has a long-range coupling to the carbonyl carbon 2. This carbon couples with proton 3, which in turn has a long-range coupling to either carbon 4. Depending on macrocycle, this carbon has either long-range couplings to aromatic protons (**5**) or to olefinic protons (**7**). The *E*- and *Z*-configurations of the macrocycle double bond were assigned based on ^{3}J couplings between the olefinic protons (15.3 Hz for *E*- and 10.3 Hz for *Z*-configuration), and by the detection of NOEs from CH_2–CH=CH protons to either both (for *E*) or only one (for *Z*) of

Table 1. Plasmepsin inhibitory activity of the prepared macrocyclic compounds

Compound	Structure	Enzyme K_i (nM)					
		Plm I	Plm II		Plm IV		Cat D
			Exp	Calcd	Exp	Calcd	
3	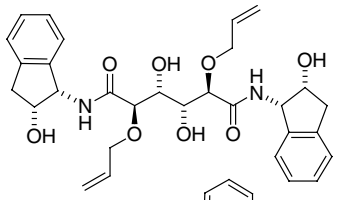	160[a]	96[b]	240[b]	>5000[c]	nd	>2000[a]
4	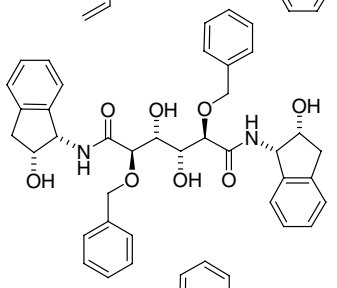	25[a]	85[a]	99[a]	nd	nd	>2000[a]
(*E*)-**5**	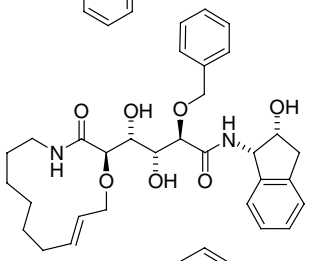	500	380	140	6800	25×10^4	>5900
6	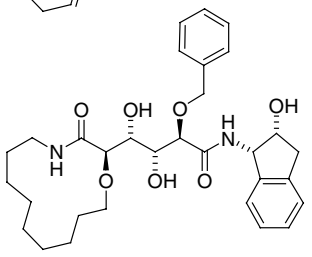	180	120	260	200	60	>5900
(*E*)-**7**	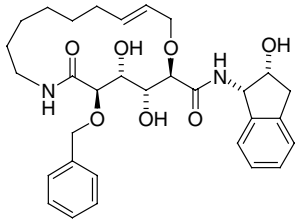	>2900	1100	2970	2000	2910	>5900
8	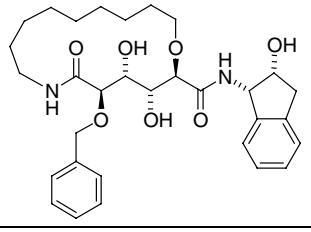	>2900	>4800	2910	2200	1460	>5900

nd, not determined.
[a] Data from Ref. 11.
[b] Data from Ref. 12.
[c] Data from Ref. 13.

the olefinic protons. Furthermore, *Z* isomers showed an NOE between allylic protons on either side of the double bond. The saturated macrocycles **6** and **8** were finally obtained by hydrogenation on Pd/C.

2.2. Enzyme inhibition

Macrocycles **5**–**8** were evaluated for their ability to inhibit the parasite Plm I, II, IV, and the human

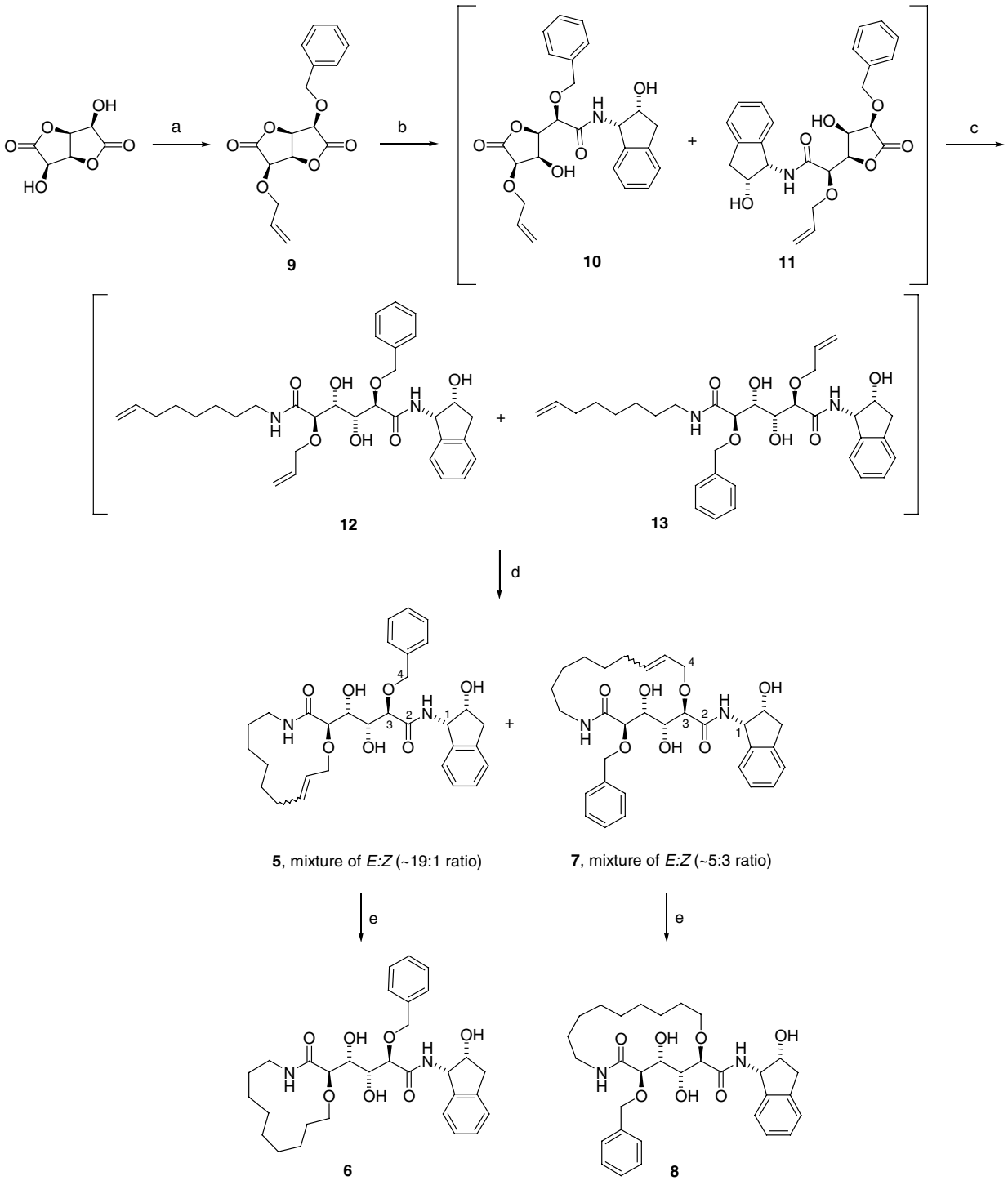

Scheme 1. Reagents and conditions: (a) 1.5 equiv benzyl trichloroacetimidate, 1.5 equiv allyl trichloroacetimidate, $BF_3 \times Et_2O$, dioxane; (b) (1*S*,2*R*)-1-amino-2-indanol, 2-hydroxypyridine, CH_2Cl_2; (c) 7-octenamine (**14**), CH_2Cl_2, reflux; (d) Grubbs catalyst second generation,[24] 1,2-dichloroethane, reflux; (e) H_2, Pd/C, MeOH.

Cat D. The results from the enzyme assays are presented as K_i values in Table 1.

Compounds **3** and **4**, used as starting points in the design, were included for comparison.[11,12] Since sufficient amounts of the pure *Z*-**5** and *Z*-**7** isomers could not be isolated, only the *E* isomers were assessed.

The 13-membered macrocycles **5** and **6** were generally much more active against the plasmepsins than the larger 16-membered macrocycles **7** and **8** with the ring spanning from the prime to the non-prime side. In fact, the 16-membered macrocycles were devoid of any inhibitory potency in the Plm I assay, and only the unsaturated **7** exhibited any potency in the Plm II assay. Overall, the

affinities toward Plm IV were low, except for the saturated 13-membered macrocycle **6**. The 13-membered saturated inhibitor **6** was significantly more potent than the unsaturated **5** in all three Plm I, II, and IV assays. In fact, compound **6** was the most potent inhibitor identified in this series, with K_i values of 180, 120, and 200 nM in the Plm I, II, and IV assays, respectively. Notably, none of the macrocycles (**5**–**8**) was active in the Cat D assay.

2.3. Computational modeling of inhibitor binding

Compounds **5**–**8** were investigated by computational procedures in order to elucidate the binding mode and to gain some insight into the molecular determinants of ligand binding. A docking exploration for each compound, in both Plm II and Plm IV enzymes, was followed by molecular dynamics (MD) coupled to an estimation of the free energy of binding with the linear interaction energy (LIE) method[25] for selected docking poses.

The docking exploration showed one consistent solution for (*E*)-**7** and **8**, the 16-membered macrocycles, in both enzymes investigated (see Figs. 2A and B). The solution positions the 16-membered ring stretching from S1′ to S2, in such a way that the amide bond present in the ring can interact with both Gly216 and the flap loop Ser79. The conformation of the 16-membered ring forces the two hydroxyls from the 1,2-dihydroxyethylene in opposite directions thereby allowing only the hydroxyl group on the non-prime side to form hydrogen bonds with the catalytic aspartic residues. The other hydroxyl group is hence strained to interact with the flap loop without the ability to establish any stable H-bond network. This arrangement of the hydroxyls stands out against our previously reported model of how the hydroxyl groups are oriented when they are not constrained in a macrocyclic system.[11,13] Further, the indanol moiety is positioned in the S2′ pocket and the benzyloxy side chain is accommodated in the S1–S3 pocket. In all cases, the docking runs converged to the aforementioned position. The stability of this binding mode for compounds (*E*)-**7** and **8** was confirmed by MD simulations. We observed frequent hydrogen bonding between the non-prime hydroxyl and the aspartates, as well as for the amide bond (with Gly36) and the hydroxyl group of the indanol moiety (with Thr192) on the prime side. The prime hydroxyl, which is pointing to the flap loop, is also involved in an internal hydrogen bond with the oxygen of the amide integrated in the macrocycle. This amide

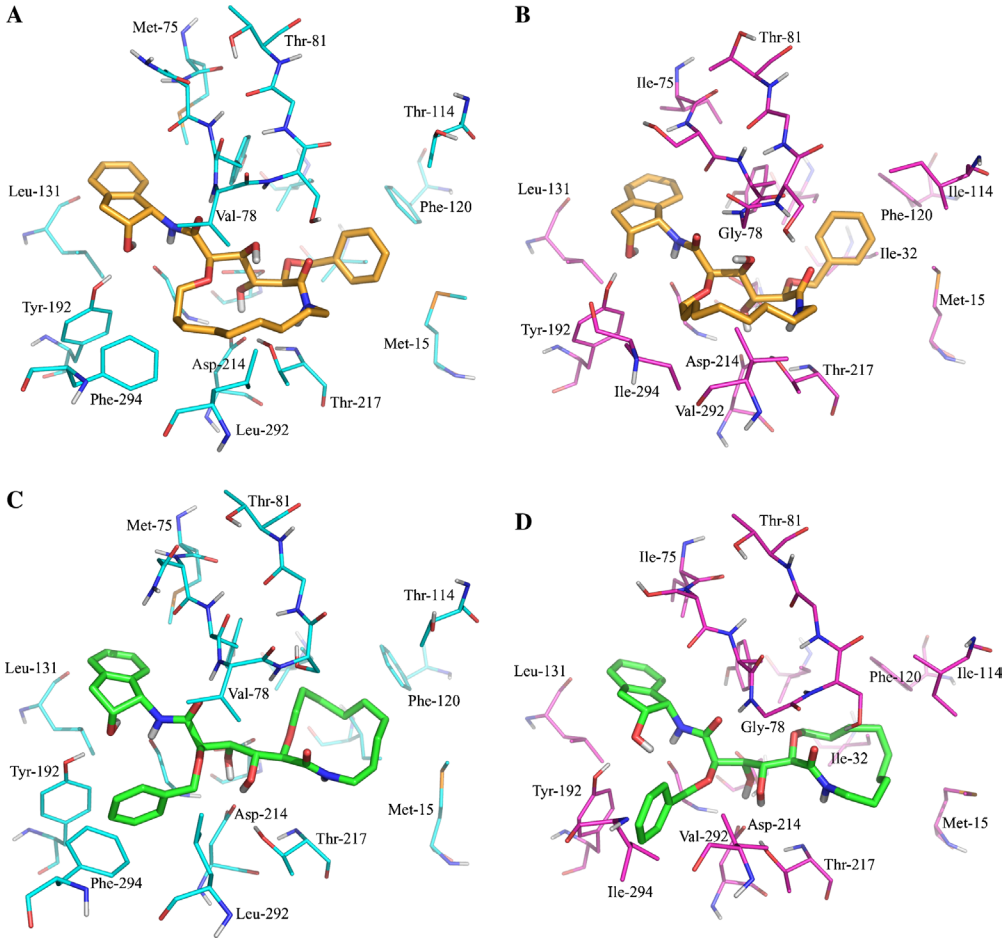

Figure 2. Binding modes of the macrocyclic compounds shown as snapshots from MD-simulations. (A and B) The 16-membered macrocyclic compound **7** in complex with Plm II and Plm IV, respectively. Analogously, (C and D) represent the 13-membered macrocycle **6** in complex with Plm II and Plm IV, respectively.

interacts with Thr217 through the NH group, after some rearrangement of the ring. In all four cases (compounds (*E*)-**7** and **8** with both Plm II and Plm IV, see Table 2), the moderate binding predicted is in excellent agreement with the experimental results.

For the 13-membered macrocycles, compounds (*E*)-**5** and **6**, the docking solutions were less consistent. In the case of Plm II, the outcome of the docking was reasonably convergent but for Plm IV there emerged several solutions. As shown in Figure 3, the proposed docking poses placed the macrocycle both in the S1–S3 binding site and in the S1′–S2′ site, while the docking position of the amino indanol and benzyloxy substituents was also not converged. Subsequently, only those solutions that showed consistency between the two enzymes were selected for further investigations. However, alternate binding modes from the Plm IV docking results, shown in Figure 3, were also examined by molecular dynamics simulations, which showed that none of them were structurally stable and that they yielded unfavorable free energies of binding (data not shown). The selected binding mode, depicted in Figures 2C and D, was consistent in the two enzymes and placed the 13-membered cycles of (*E*)-**5** and **6** in the S1–S3 cleft. The two central hydroxyls were positioned at hydrogen-bond distances to the catalytic aspartic acids in a manner consistent with previous studies.[11–13] The amino indanol group was found in the S2′ site, analogously to what was found for compounds (*E*)-**7** and **8**. Finally, the benzyloxy side chain was in this case placed into the S1′ pocket as opposed to (*E*)-**7** and **8**, where the benzyloxy substituent was placed in S1. Molecular dynamics showed high stability for the interactions involved in the aforementioned position for both (*E*)-**5** and **6** when bound to Plm II. The same stability was found as well for the saturated compound **6** in Plm IV, with binding free energy estimates in excellent agreement with experimental measurements (see Table 2). However, for the unsaturated compound (*E*)-**5**, the binding conformation adopted in Plm IV by the more rigid macrocycle forced the hydroxyl groups to be positioned in a non-optimal geometry for the hydrogen bonding to the catalytic aspartates. This caused a dramatic decrease in the predicted affinity, an observation that is in agreement with the experimental evidences although somewhat exaggerated.

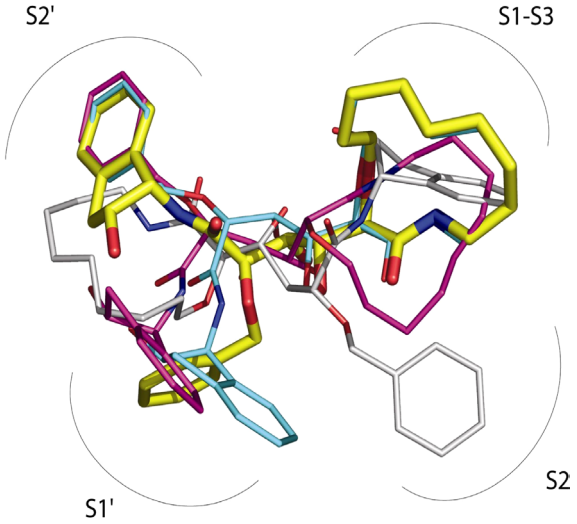

Figure 3. Alternative docking poses found for compound **6** into Plm IV by GOLD. The pose selected for further evaluations, here shown in thick yellow sticks, was also obtained in Plm II docking experiments.

3. Discussion

Two of our previously reported linear inhibitors, **3** and **4**, originating from mannitol and containing a 1,2-dihydroxyethylene motif, are shown in Table 1.[12] Within this class of inhibitors several compounds with high affinity for both Plm I and II, and with a remarkable selectivity over the human Cat D were identified.[12] By utilizing the ring-closing metathesis (RCM) methodology these inhibitors were constrained, providing either a 13-membered (unsaturated **5** and saturated **6**) or a 16-membered (unsaturated **7** and saturated **8**) macrocycle. As compared to **3** and **4**, the new compounds are lacking one of the two indanol groups, and in relation to **4** one of the benzyloxy side chains. As can be seen in Table 1, the smaller 13-membered macrocycles (*E*)-**5** and **6** were in general significantly more potent against Plm I, II, and IV than the 16-membered cycles (*E*)-**7** and **8** bridging the prime to the non-prime side. According to previous observations,[19,21] this effect might be attributed to the variation on position 78 at the tip of the flap; Plm I and II both possessing a sterically demanding valine, which in Plm IV is replaced by a glycine. In addition, it was evident that the constrained macrocycles imposed

Table 2. Experimental and calculated free energies of binding for compounds **5**–**8** in both Plm II and Plm IV

Enzyme	Compound	$\Delta G_{\text{bind, exp}}$(kcal/mol)[a]	$\Delta G_{\text{bind, calcd}}$ (kcal/mol)	Ligand–surrounding interactions (kcal/mol)[b]			
				$\langle V_{\text{l–s}}^{\text{vdW}}\rangle_{\text{p}}$	$\langle V_{\text{l–s}}^{\text{el}}\rangle_{\text{p}}$	$\langle V_{\text{l–s}}^{\text{vdW}}\rangle_{\text{w}}$	$\langle V_{\text{l–s}}^{\text{el}}\rangle_{\text{w}}$
Plm II	(*E*)-**5**	−8.8	−9.4 ± 1.2	−66.3 ± 0.3	−84.3 ± 1.8	−42.7 ± 0.2	−68.7 ± 1.5
	6	−9.5	−9.1 ± 0.8	−64.0 ± 0.2	−85.3 ± 0.5	−43.7 ± 0.6	−69.0 ± 1.4
	(*E*)-**7**	−8.2	−7.6 ± 1.4	−64.7 ± 2.9	−83.5 ± 0.6	−43.8 ± 0.3	−72.0 ± 1.9
	8	>−7.3	−7.6 ± 1.0	−65.7 ± 0.3	−80.1 ± 1.7	−43.7 ± 0.2	−69.1 ± 1.0
Plm IV	(*E*)-**5**	−7.1	−4.9 ± 0.7	−72.1 ± 0.9	−67.6 ± 0.1	−42.7 ± 0.2	−68.7 ± 1.5
	6	−9.2	−9.9 ± 1.3	−74.8 ± 0.3	−82.0 ± 2.1	−43.7 ± 0.6	−69.0 ± 1.4
	(*E*)-**7**	−7.8	−7.6 ± 1.6	−72.5 ± 0.8	−79.3 ± 2.3	−43.8 ± 0.3	−72.0 ± 1.9
	8	−7.8	−8.0 ± 0.6	−75.8 ± 0.6	−75.8 ± 0.6	−43.7 ± 0.2	−69.1 ± 1.0

[a] The experimental binding free energy calculated from experimentally determined K_i's using $\Delta G^0_{\text{bind,exp}} = RT \ln K_i$.

[b] The calculated average electrostatic $\langle V_{\text{el}}\rangle$ and non-polar $\langle V_{\text{vdW}}\rangle$ energies for ligand–surrounding (l–s) interactions. The subscripts p and w denote simulations of the ligand in complex with the protein and free in water, respectively.

an unfavorable position of the crucial hydroxyl groups in the central transition state mimicking core unit. The saturated 13-atom macrocycle **6** constitutes the most potent plasmepsin inhibitor obtained in the series. This inhibitor was about three times as active against Plm I and II, and over 30 times as active against Plm IV as the corresponding unsaturated inhibitor **5**, possibly reflecting an increased flexibility upon saturation enabling a proper adaptation of the compound in the enzyme active site. Additionally, inhibitor **6** was over 25-fold more potent against Plm IV and almost equipotent against Plm I and II compared to the parent linear inhibitor **3**. Considering that the P2 side chain is omitted from the 13-membered inhibitors and that a considerable selectivity versus the human Cat D could be achieved, this suggests macrocyclization as a viable strategy for further optimization.

Docking experiments with Plm II and Plm IV indicated that the 16-membered macrocycles in (*E*)-**7** and **8** are aligned along the S1′–S2 subsites, while the 13-membered cycles of (*E*)-**5** and **6** are located in the S1–S3 cleft. The feasibility of these docking poses was confirmed by binding free energy estimations using the linear interaction energy approach, obtaining a reasonable agreement between calculated and experimental binding constants. It is interesting to note that the introduction of the double bond in the 13 member macrocycle (compounds (*E*)-**5** and **6**) leads to a 30-fold drop in affinity for Plm IV, a trend that is reproduced in our computational model. The common hypothesis that rigid analogues, through a lower loss of conformational entropy upon binding, have a free energy advantage relative to their flexible counterparts[26] is not obeyed in this case. On the contrary, our simulations show that the double bond present in compound (*E*)-**5** leads to a non-optimal match to the Plm IV pocket compared to the more flexible inhibitor **6**, as highlighted in Figure 4. The difference between the two related compounds, although overestimated by the binding affinity calculations, originates from an unfavorable arrangement of the *E* isomer ring in the S1–S3 pocket (see Fig. 4). Even if the docking solutions for the saturated and unsaturated compounds are almost identical, after some MD we observed a conformational rearrangement of the unsaturated compound. The new, slightly modified position remained stable for the rest of the data collection trajectory and had a pronounced effect on the interface between the inhibitor and the enzyme close to the catalytic residues, as shown in Figure 4. Compared to Plm II, the S1–S3 pocket in Plm IV has more restricted geometrical bounds, identified by the mutation at position 114 from Thr in Plm II to the more bulky Ile in Plm IV. For the saturated compound we did not observe significant differences between the two enzymes, indicating that a flexible ring is more likely to adapt to the geometrical restraints of the enzyme.

The initial docking results of the 16-membered ring compounds initially pointed to the hypothesis that Val78 in Plm II constitutes a larger steric obstacle than Gly78 in Plm IV. However, after the equilibration period in the MD simulations, both binding sites seem to accommodate the macrocycle equally well, as shown in Figures 2A and B. In fact, the loss in affinity due to the S1′–S2 macrocyclization is equivalent in both enzymes. The initially more closed surface of Plm II is compensated by a relaxation of the backbone of the flap loop, and an almost perfect superposition of the ligand can be observed if the two complexes are compared. It should be noted, however, that the shape complementarity is not optimal in either of the enzymes for (*E*)-**7** and **8**, leading to structural fluctuations of the macrocyclic rings. We even observe some partial flap loop opening during our simulations due to such fluctuations. A second common factor responsible for the weaker binding of the larger cycles is found in the orientation of the 1,2-hydroxyethylene hydroxyls enforced by the conformational restraints of the macrocycle. Only one of the two core hydroxyl groups is able to interact with the catalytic aspartic acid residues, while the other is left to interact with the loop and to make an internal hydrogen bond with an amide bond of the macrocycle. This interaction profile appears less favorable compared to the

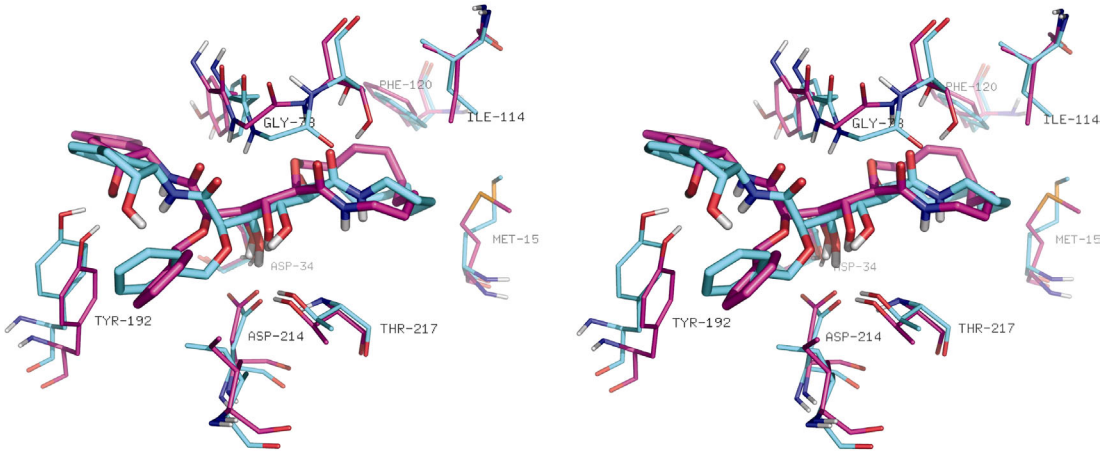

Figure 4. Corss-eyed stereo view of (*E*)-**5** (light blue) and **6** (magenta) in complex with Plm IV. Relevant snapshots were extracted from MD trajectories. Only residues in close contact with the ligands are depicted, and water molecules have been removed. The conformation adopted by the cycle upon binding is not the same in the two compounds, leading to different geometry of the protein–ligand interactions.

hydrogen bonding pattern observed in the 13-membered ring compounds, consistent with previously reported inhibitors.[11–13]

The previously reported inhibitors comprising a macrocycle element did not exhibit any selectivity for the plasmepsins over the human aspartic protease Cat D.[19] Since the linear 1,2-dihydroxyethylene-based inhibitors have shown a considerable selectivity over Cat D, they appeared to provide good starting points in the search for selective macrocyclic inhibitors. In agreement with this hypothesis, none of the macrocyclic 1,2-dihydroxyethylene compounds inhibited Cat D.

4. Conclusion

Inhibitors encompassing 13-membered and 16-membered macrocyclic ring structures and that inhibit *P. falciparum* Plm I, II, and IV have been synthesized. Cyclization was accomplished by means of RCM using Grubbs second generation catalyst. The binding mode of this new class of compounds was predicted by molecular modeling, leading to a consistent interpretation of the experimental results. One saturated 13-membered macrocyclic compound (**6**) was found with an equally high affinity for all three plasmepsins (Plm I, II, and IV). This compound exerted no activity in the Cat D assay. To the best of our knowledge, these compounds are the first macrocyclic plasmepsin inhibitors that exhibit a high selectivity for the plasmepsins over the human Cat D.

5. Experimental

5.1. Chemistry

5.1.1. General information. NMR spectra were recorded on a JEOL JNM-EX400 spectrometer (^{1}H at 399.8 MHz and ^{13}C at 100.5 MHz), a Varian UNITY INOVA spectrometer (^{1}H at 499.9 MHz), a Varian UNITY spectrometer (^{1}H at 399.5 MHz) or on a Varian Mercury Plus spectrometer (^{1}H at 300.0 MHz, ^{13}C at 75.4 MHz). Chemical shifts are reported as δ values (ppm) indirectly referenced to TMS via the solvent residual signal. Two-dimensional (2D) HMBC spectra were recorded on a Varian UNITY INOVA spectrometer (^{1}H at 499.9 MHz) or on a Varian Mercury Plus spectrometer (^{1}H at 300.0 MHz) using standard pulse sequences. NOE effects were recorded on a Varian UNITY INOVA spectrometer (^{1}H at 499.9 MHz) or on a Varian UNITY spectrometer (^{1}H at 399.5 MHz) using a NOESY experiment with a mixing time of 0.8 s. Optical rotations were obtained on a Perkin-Elmer 241 polarimeter. Specific rotations ($[\alpha]_D$) are reported in deg/dm, and the concentration (c) is given in g/100 mL in the specified solvent. Elemental analyses were performed by Analytische Laboratorien, Lindlar, Germany. Flash chromatography was performed on Merck silica gel 60, 0.04–0.063 mm. Analytical RP-LC–MS was performed on a Gilson HPLC system with a C18 (Merck KgaA Chromolith Performance RP-18e (4.6 × 100 mm)) column, with a Finnigan AQA quadropole mass spectrometer, at a flow rate of 4 mL/min, using different gradients of CH_3CN in 0.05% aqueous formic acid. Preparative RP-LC–MS was performed on a Gilson HPLC system with either a C8 (Agilent Technologies Zorbax SB-C8 (5 μm, 21.2 × 150 mm)) column or a C18 (YMC ODS-AQ (5 μm, 20 × 50 mm)) column, with a Finnigan AQA quadropole mass spectrometer, at a flow rate of 15 mL/min, using different gradients of CH_3CN in 0.05% aqueous formic acid.

5.1.2. 2-*O*-Allyl-5-*O*-benzyl-L-mannaro-1,4:3,6-di-γ-lactone (9). L-1,4:3,6-Mannarodilactone (1.0 g, 5.7 mmol) was dissolved in dry dioxane (130 mL) under a nitrogen atmosphere. To the stirred solution were added benzyl trichloroacetimidate (2.2 g, 8.6 mmol), allyl trichloroacetimidate (1.8 g, 8.6 mmol), and a catalytic amount of $BF_3 \times OEt_2$ (590 μL). The solution was stirred at room temperature for 3 h. After filtration through a silica pad, the filtrate was concentrated under reduced pressure. The crude product was washed with diethyl ether (2 × 30 mL) to give a mixture of **9** together with the two dialkylated molecules 2,5-di-*O*-allyl-L-mannaro-1,4:3,6-di-γ-lactone and 2,5-di-*O*-benzyl-L-mannaro-1,4:3,6-di-γ-lactone (in a total of 1.2 g). In general, this mixture was used in the next step without further purification. A small portion (100 mg) was purified on RP-LC (C8 column, 30 min gradient of 35-80% CH_3CN in 0.05% aqueous formic acid) to yield pure compound **9** (29 mg), which was analyzed: $[\alpha]_D^{19}$ −159.8 (*c* 1.00, CH_3CN); ^{1}H NMR (399.8 MHz; $CD_3OD/CDCl_3$, 2:7) δ 7.38–7.25 (m, 5H), 5.89 (ddt, J = 17.2, 10.3, 6.1, Hz, 1H), 5.32 (dm, J = 17.2 Hz, 1H), 5.25 (dm, J = 10.3 Hz, 1H), 4.98 (dd, J = 3.2, 4.7 Hz, 1H), 4.89 (dd, J = 3.2, 4.8 Hz, 1H), 4.84 (d, J = 12.0 Hz, 1H), 4.79 (d, J = 12.0 Hz, 1H), 4.39 (d, J = 4.7 Hz, 1H), 4.36 (d, J = 4.8 Hz, 1H), 4.33–4.19 (m, 2H); ^{13}C NMR (100.5 MHz; $CD_3OD/CDCl_3$, 2:7) δ 170.8 (2C, according to HMBC), 135.7, 132.7, 128.6, 128.5, 128.3, 119.7, 74.0, 73.92, 73.89, 73.8, 72.9, 72.2. Anal. ($C_{16}H_{16}O_6$) C, H.

5.1.3. 7-Octenamine (14). 8-Bromo-1-octene (2.5 g, 13.1 mmol) and sodium azide (936 mg, 14.4 mmol) were dissolved in EtOH (16 mL) and stirred at reflux for 16 h. The solvent was removed under reduced pressure. The crude product was partitioned between CH_2Cl_2 (100 mL) and H_2O (100 mL). The aqueous layer was extracted with CH_2Cl_2 (2 × 100 mL) and the combined organic layers were dried (Na_2SO_4) and concentrated. A solution of the crude azide (2.0 g, 13.1 mmol) in dry diethyl ether (30 mL) was added drop-wise to a stirred mixture of $LiAlH_4$ (993 mg, 26.2 mmol) in dry diethyl ether (50 mL) at 0 °C. The mixture was allowed to attain room temperature, stirred for 3 h, and then quenched by the addition of H_2O (2 mL), 15% NaOH (2 mL), and more H_2O (6 mL), followed by filtration. The mixture was diluted with H_2O (80 mL) and diethyl ether (30 mL). The organic layer was separated and the aqueous layer was extracted with diethyl ether (2 × 100 mL) and CH_2Cl_2 (3 × 100 mL). The combined organic layers were dried (Na_2SO_4) and concentrated to yield the amine **14** (1.2 g, 72%).[27]

5.1.4. Mixture of (2*R*)-1*N*-(2-hydroxyindan-1-yl)-2-benzyloxy-2-[(2*R*,3*R*,4*R*)-4-(2-propenyloxy)-3-hydroxy-5-oxo-tetrahydrofuran-2-yl]-ethanamide (10) and (2*R*)-1*N*-(2-hydroxyindan-1-yl)-2-(2-propenyloxy)-2-[(2*R*,3*R*,4*R*)-4-benzyloxy-3-hydroxy-5-oxo-tetrahydrofuran-2-yl]-ethanamide (11). The bislactone mixture of **9** together with 2,5-di-*O*-allyl-L-mannaro-1,4:3,6-di-γ-lactone and 2,5-di-*O*-benzyl-L-mannaro-1,4:3,6-di-γ-lactone) (2.0 g) and 2-hydroxypyridine (540 mg, 5.7 mmol) were dissolved in dry CH_2Cl_2 (140 mL) and stirred at room temperature for 30 min. The solution was cooled to 0 °C and (1*S*,2*R*)-1-amino-2-indanol (846 mg, 5.7 mmol) was added rapidly. The reaction mixture was allowed to attain room temperature and stirred overnight for 12 h. The solvent was removed under reduced pressure and subsequent flash chromatography ($CHCl_3$) gave a mixture of the two variants of mono-opened bislactones **10** and **11** (501 mg). As **10** and **11** could not be completely separated from each other, the mixture was used in the next step without further purification.

5.1.5. Mixture of (2*R*,3*R*,4*R*,5*R*)-2-benzyloxy-3,4-dihydroxy-*N*1-[(1*S*,2*R*)-2-hydroxyindan-1-yl]-*N*6-(7-octene)-5-(2-propenyloxy)-hexanamide (12) and (2*R*,3*R*,4*R*,5*R*)-5-benzyloxy-3,4-dihydroxy-*N*1-[(1*S*,2*R*)-2-hydroxyindan-1-yl]-*N*6-(7-octene)-2-(2-propenyloxy)-hexanamide (13). The mixture of the two variants of mono-opened bislactone **10** and **11** (167 mg, 0.37 mmol) was dissolved in dry CH_2Cl_2 (4 mL) and 7-octenamine (235 mg, 1.8 mmol) was added. The reaction mixture was stirred at reflux for 3 h. The solvent was removed under reduced pressure and subsequent purification by RP-LC–MS (C8 column, 30 min gradient of 30–90% CH_3CN in 0.05% aqueous formic acid) gave a mixture of the two diamides **12** and **13** (157 mg, 73%). As **12** and **13** could not be separated from each other, the mixture was used in the next step without further purification.

5.1.6. (2*R*,3*R*,4*R*)-2-Benzyloxy-3,4-dihydroxy-*N*-[(1*S*,2*R*)-2-hydroxyindan-1-yl]-4-[(2*R*)-3-oxo-1-oxa-4-aza-cyclotridec-11-en-2-yl]-butyramide (5) and (2*R*,3*R*,4*R*,5*R*)-5-benzyloxy-3,4-dihydroxy-6-oxo-1-oxa-7-aza-cyclohexadec-14-ene-2-carboxylic acid [(1*S*,2*R*)-2-hydroxyindan-1-yl]-amide (7). The mixture of the diamides **12** and **13** (58 mg, 0.10 mmol) was dissolved in dry 1,2-dichloroethane (20 mL) and a second generation Grubbs catalyst (benzylidene[1,3-bis(2,4,6-trimethylphenyl)-2-imidazolidinylidene]dichloro-(tricyclohexylphosphine)ruthenium) (8.5 mg, 0.010 mmol) was added. Since the reaction was slow, additional amounts of second-generation Grubbs catalyst were added (4.2 mg, 0.0050 mmol and 4.2 mg, 0.0050 mmol after 2 and 4 h, respectively). The reaction mixture was stirred at reflux for 6 h. The solvent was removed under reduced pressure and subsequent purification on RP-LC–MS (C18 column, 30 min gradient of 25–65% CH_3CN in 0.05% aqueous formic acid) gave the *E*- and *Z*-diastereomers of the two different macrocycles **5** and **7** (in a total of 26.3 mg, 48%) as white solids. (E/Z)-5. ^{1}H NMR (499.9 MHz; $CD_3OD/CDCl_3$, 3:1) of the LC–MS purified mixture was used to estimate the E/Z ratio of **5** to ~19:1. (*E*/*Z*)-7. ^{1}H NMR (499.9 MHz; $CD_3OD/CDCl_3$, 3:1) of the LC–MS purified mixture was used to estimate the *E*/*Z* ratio of **7** to ~5:3.

5.1.7. (2*R*,3*R*,4*R*)-2-Benzyloxy-3,4-dihydroxy-*N*-[(1*S*,2*R*)-2-hydroxyindan-1-yl]-4-[(2*R*,11*E*)-3-oxo-1-oxa-4-aza-cyclotridec-11-en-2-yl]-butyramide ((*E*)-5). $[\alpha]_D^{18}$ −24.8 (*c* 0.79, $CHCl_3$); ^{1}H NMR (499.9 MHz; acetone-d_6/C_6D_6, 2:1) δ 7.85 (d, *J* = 8.7 Hz, 1H), 7.46–7.25 (m, 9 H), 5.84 (dddm, *J* = 15.3, 7.2, 7.2 Hz, 1H), 5.73 (dddm, *J* = 7.0, 7.0, 15.3 Hz, 1H), 5.57 (dd, *J* = 5.1, 8.7 Hz, 1H), 5.24 (s, 1H), 5.98 (s, 1H), 4.84 (d, *J* = 11.4 Hz, 1H), 4.80 (d, *J* = 11.4 Hz, 1H), 4.73 (ddm, *J* = 5.1, 5.1 Hz, 1H), 4.52 (s, 1H), 4.45 (d, *J* = 7.3 Hz, 1H), 4.35 (ddm, *J* = 12.6, 7.2 Hz, 1H), 4.29 (dm, *J* = 7.3 Hz, 1H), 4.22 (dm, *J* = 7.7 Hz, 1H), 4.13 (d, *J* = 7.7 Hz, 1H), 4.06 (ddm, *J* = 12.6, 7.2 Hz, 1H), 3.67 (m, 1H), 3.17 (dd, *J* = 5.1, 16.2 Hz, 1H), 3.08–2.98 (m, 2H), 2.20–2.08 (m, 2H), 1.77 (m, 1H), 1.56–1.34 (m, 7H). A NOESY (499.9 MHz) experiment confirmed the *E* geometry of the double bond, and an HMBC (499.9 MHz) experiment confirmed the size of the macrocycle; ^{13}C NMR (75.4 MHz; $CDCl_3$) δ 173.0, 172.7, 141.0, 140.1, 138.6, 137.0, 128.9, 128.6, 128.55, 128.50, 127.3, 126.3, 125.6, 124.3, 81.4, 80.5, 74.1, 73.9, 72.9, 71.9, 71.8, 58.2, 39.6, 38.4, 31.3, 26.3, 25.9, 25.3, 23.6. Anal ($C_{31}H_{42}N_2O_7 \cdot 1/3H_2O$) C, H, N.

5.1.8. (2*R*,3*R*,4*R*)-2-Benzyloxy-3,4-dihydroxy-*N*-[(1*S*,2*R*)-2-hydroxyindan-1-yl]-4-[(2*R*,11*Z*)-3-oxo-1-oxa-4-aza-cyclotridec-11-en-2-yl]-butyramide ((*Z*)-5). ^{1}H NMR (499.9 MHz; $CD_3OD/CDCl_3$, 3:1) δ 7.40–7.14 (m, 9H), 5.57 (dm, *J* = 10.3 Hz, 1H), 5.47 (dm, *J* = 10.3 Hz, 1H), 5.36 (d, *J* = 5.0 Hz, 1H), 4.67 (d, *J* = 11.4 Hz, 1H), 4.64 (d, *J* = 11.4 Hz, 1H), 4.59 (ddd, *J* = 1.7, 5.0, 5.1 Hz, 1H) 4.18–4.14 (m, 3H), 4.07 (dd, *J* = 2.1, 6.6 Hz, 1H), 3.98 (dd, *J* = 2.1, 7.6 Hz, 1H), 3.95 (d, *J* = 7.6 Hz, 1H), 3.35 (m, 1H), 3.23–3.12 (m, 2H), 2.94 (dd, *J* = 1.7, 16.6 Hz, 1H), 2.22 (m, 1H), 2.02–1.94 (m, 1H), 1.75 (m, 1H), 1.50–1.24 (m, 7H). A NOESY (499.9 MHz) experiment confirmed the *Z* geometry of the double bond, and an HMBC (499.9 MHz) experiment confirmed the size of the macrocycle.

5.1.9. (2*R*,3*R*,4*R*,5*R*,14*E*)-5-Benzyloxy-3,4-dihydroxy-6-oxo-1-oxa-7-aza-cyclohexadec-14-ene-2-carboxylic acid [(1*S*,2*R*)-2-hydroxyindan-1-yl]-amide ((*E*)-7). $[\alpha]_D^{18}$ +11.6 (*c* 0.69, CH_2Cl_2); ^{1}H NMR (499.9 MHz; $CD_3OD/CDCl_3$, 3:1) δ 7.39–7.18 (m, 9H), 5.70 (dddm, *J* = 7.0, 7.0, 15.3 Hz, 1H), 5.58 (dddm, *J* = 6.0, 6.0, 15.3 Hz, 1H), 5.37 (d, *J* = 5.0 Hz, 1H), 4.63–4.57 (m, 3H), 4.22 (ddd, *J* = 1.2, 6.0, 12.5 Hz, 1H), 4.07–4.03 (m, 2H), 4.01 (d, *J* = 6.8 Hz, 1H), 3.96 (dd, *J* = 2.0, 6.8 Hz, 1H), 3.89 (ddd, *J* = 1.1, 6.0, 12.5 Hz, 1H), 3.46 (ddd, *J* = 3.2, 8.3, 13.6 Hz, 1H), 3.16 (dd, *J* = 5.1, 16.6 Hz, 1H), 3.08 (ddd, *J* = 3.2, 7.8, 13.6 Hz, 1H), 2.95 (dd, *J* = 1.8, 16.6 Hz, 1H), 2.10–2.04 (m, 2H), 1.61 (m, 1H), 1.51–1.25 (m, 7H). A NOESY (399.5 MHz) experiment confirmed the *E* geometry of the double bond, and an HMBC (499.9 MHz) experiment confirmed the size of the macrocycle; ^{13}C NMR (75.4 MHz; $CD_3OD/CDCl_3$, 3:1) δ 174.1, 173.7, 141.7, 141.4, 138.2, 136.4, 129.37, 129.28, 129.0, 128.9, 127.8, 126.7, 126.1, 125.1, 80.9, 79.8, 74.0, 73.7, 72.7, 72.4, 71.8, 58.3, 40.6, 39.6, 32.1, 29.5, 29.3, 28.7, 27.7. Anal ($C_{31}H_{42}N_2O_7 \cdot 1/3H_2O$) C, H, N.

5.1.10. (2*R*,3*R*,4*R*,5*R*,14*Z*)-5-Benzyloxy-3,4-dihydroxy-6-oxo-1-oxa-7-aza-cyclohexadec-14-ene-2-carboxylic acid [(1*S*,2*R*)-2-hydroxyindan-1-yl]-amide ((*Z*)-7). ^{1}H NMR

(499.9 MHz; $CD_3OD/CDCl_3$, 3:1) δ 7.39–7.18 (m, 9H), 5.61–5.51 (m, 2H), 5.37 (d, $J = 5.0$ Hz, 1H), 4.67–4.57 (m, 3H), 4.29 (ddm, $J = 8.2$, 10.1 Hz, 1H), 4.08 (dd, $J = 1.6$, 7.7 Hz, 1H), 4.03–3.97 (m, 4H), 3.95 (dd, $J = 1.6$, 7.6 Hz, 1H), 3.58 (ddd, $J = 3.2$, 9.5, 13.4 Hz, 1H), 3.17 (dd, $J = 5.0$, 16.6 Hz, 1H), 3.02 (ddd, $J = 3.3$, 6.3, 13.4 Hz, 1H), 2.95 (dd, $J = 1.5$, 16.6 Hz, 1H), 2.27 (m, 1H), 2.01 (m, 1H), 1.63–1.24 (m, 8H). A NOESY (499.9 MHz) experiment confirmed the *Z* geometry of the double bond, and an HMBC (499.9 MHz) experiment confirmed the size of the macrocycle.

5.1.11. (2*R*,3*R*,4*R*)-2-Benzyloxy-3,4-dihydroxy-*N*-[(1*S*,2*R*)-2-hydroxyindan-1-yl]-4-[(2*R*)-3-oxo-1-oxa-4-aza-cyclotridec-2-yl]-butyramide (6). The mixture of *E* and *Z* isomers of **5** (9.5 mg, 0.017 mmol) was dissolved in MeOH (4 mL) and palladium 10 wt% (dry basis, 50% water) on activated carbon (2 mg) was added. The reaction mixture was stirred under H_2 at room temperature for 3 h. The palladium on carbon was filtered off and the filtrate was concentrated under reduced pressure. Purification using RP-LC (C8 column, 30 min gradient of 30–80% CH_3CN in 0.05% aqueous formic acid) gave the saturated macrocycle **6** (5.9 mg, 62%) as a white solid: $[\alpha]_D^{18}$ +20.3 (*c* 0.81, $CHCl_3$); ^1H NMR (300.0 MHz; $CD_3OD/CDCl_3$, 3:1) δ 7.38–7.16 (m, 9H), 5.35 (d, $J = 5.1$ Hz, 1H), 4.69 (d, $J = 11.4$ Hz, 1H), 4.64 (d, $J = 11.4$ Hz, 1H), 4.56 (ddd, $J = 1.7$, 5.1, 5.1 Hz, 1H), 4.18 (d, $J = 6.3$ Hz, 1H), 4.03 (dd, $J = 2.3$, 6.3 Hz, 1H), 3.99 (dd, $J = 2.3$, 7.2 Hz, 1H), 3.85 (d, $J = 7.2$ Hz, 1H), 3.74 (m, 1H), 3.58–3.36 (m, 2H), 3.26–3.10 (m, 2H), 2.93 (dd, $J = 1.7$, 16.7 Hz, 1H), 1.78–1.1.62 (m, 2H), 1.57–1.23 (m, 12H); ^{13}C NMR (75.4 MHz; $CD_3OD/CDCl_3$, 3:1) δ 174.0, 173.6, 141.43, 141.35, 138.1, 129.3, 129.2, 128.94, 128.92, 127.8, 126.0, 125.1, 82.1, 81.4, 74.0, 73.6, 71.74, 71.66, 71.5, 58.3, 40.5, 39.1, 29.2, 26.9, 25.9, 25.5, 23.9, 23.6. One ^{13}C signal is missing in the aliphatic area due to overlapping resonances. When changing solvent to pure $CDCl_3$, all of the aliphatic signals were split into separate signals. Anal ($C_{31}H_{42}N_2O_7$) C, H, N.

5.1.12. (2*R*,3*R*,4*R*,5*R*)-5-Benzyloxy-3,4-dihydroxy-6-oxo-1-oxa-7-aza-cyclohexadec-2-carboxylic acid [(1*S*,2*R*)-2-hydroxyindan-1-yl]-amide (8). The mixture of *E* and *Z* isomers of **7** (8.6 mg, 0.016 mmol) was dissolved in MeOH (4 mL) and palladium 10 wt% (dry basis, 50% water) on activated carbon (2 mg) was added. The reaction mixture was stirred under H_2 at room temperature for 3 h. The palladium on carbon was filtered off and the filtrate was concentrated under reduced pressure. Purification using RP-LC (C8 column, 30 min gradient of 30–80% CH_3CN in 0.05% aqueous formic acid) gave the saturated macrocycle **8** (5.2 mg, 60%) as a white solid: $[\alpha]_D^{18}$ +9.8 (*c* 1.2, CH_2Cl_2); ^1H NMR (300.0 MHz; CD_3OD) δ 7.45–7.17 (m, 9H), 5.41 (d, $J = 4.8$ Hz, 1H), 4.66–4.55 (m, 3H), 4.10 (dd, $J = 1.3$, 9.1 Hz, 1H), 4.01–3.93 (m, 2H), 3.90 (d, $J = 8.8$ Hz, 1H), 3.73 (m, 1H), 3.62 (ddd, $J = 3.1$, 8.9, 13.3 Hz, 1H), 3.46 (m, 1H), 3.19 (dd, $J = 5.0$, 16.6 Hz, 1H), 3.02–2.91 (m, 2H), 1.67–1.24 (m, 14H); ^{13}C NMR (75.4 MHz; $CD_3OD/CDCl_3$, 3:1) δ 174.64, 174.60, 141.7, 141.3, 138.1, 129.34, 129.28, 129.0, 128.9, 127.8, 126.1, 125.1, 80.5 (2C, according to HMBC), 74.5, 73.7, 72.5, 71.4, 71.2, 58.2, 40.7, 39.6, 30.2, 30.0, 29.6, 28.8, 28.1, 26.7, 26.5. Anal ($C_{31}H_{42}N_2O_7 \cdot 2H_2O$) C, H, N.

5.1.13. Enzyme assays. Plm II was prepared according to Westling et al.[28], and the expression and purification of Plm I will be published elsewhere (manuscript in preparation). The Plm IV assay was performed as described elsewhere.[29] Human liver Cat D was purchased from Sigma–Aldrich, Sweden. The activities of Plm I, Plm II, and Cat D were measured essentially as described earlier,[30] using a total reaction volume of 100 μL. The concentration of pro-Plm II was 3 nM, the amount of Plm I was adjusted to give a similar catalytic activity, and 50 ng/mL pro-Cat D was used. The pro-sequence of Plm II was cleaved off by preincubation in assay reaction buffer (100 mM sodium acetate buffer (pH 4.5), 10% glycerol, and 0.01% Tween 20) at room temperature for 40 min, and Cat D was activated by incubation in the same reaction buffer at 37 °C for 20 min. The reaction was initiated by the addition of 3 μM substrate (DABCYL-Glu-Arg-Nle-Phe-Leu-Ser-Phe-Pro-EDANS, AnaSpec Inc, San Jose, CA, USA) and hydrolysis was recorded as the increase in fluorescence intensity over a 10-min time period, during which the rate increased linearly with time. Stock solutions of inhibitors in DMSO were serially diluted in DMSO and added directly before addition of the substrate, giving a final DMSO concentration of 1%. IC_{50} values were obtained by assuming competitive inhibition and fitting the Langmuir isotherm ($v_i/v_o = 1/(1 + [I]/IC_{50})$) to the dose–response data (Grafit), where v_i and v_o are the initial velocities of the inhibited and uninhibited reactions, respectively, and [I] is the inhibitor concentration.[31] K_i was subsequently calculated using $K_i = IC_{50}/(1 + [S]/K_m)$[32] and a K_m value was determined according to Michaelis–Menten.

5.1.14. Computational modeling. Compounds **5**–**8** were built in an extended conformation with the program ViewerPro,[33] while the coordinates of the plasmepsins investigated were retrieved from the Bookhaven Databank[34] (codes 1LF2 and 1LF3 for Plm II and 1LS5 for Plm IV) with subsequent addition of hydrogens. Regarding the catalytic aspartates, Asp34 was considered protonated and Asp214 negatively charged, according to our previous works.[11] Docking was performed with GOLD v2.2,[35] allowing full flexibility for the ligand, while keeping the protein fixed. The following protocol was used to explore the three crystallographic structures mentioned above: 20 independent runs of the docking algorithm were performed with each compound, using the default genetic algorithm (GA) search parameters but increasing the number of operators that are applied over the course of a GA run to 300.000. Both the Goldscore and Chemscore scoring functions implemented in GOLD[36] were used in parallel assays on each compound. The automated assignment of protein and ligand atom types was checked in order to ensure the correct treatment of the potential hydrogen bond donors and acceptors.

Binding free energies were estimated with the linear interaction energy (LIE) method, described in detail

elsewhere.[25,37] Basically, this approach estimates the ligand free energy of binding from the difference in the ligand surrounding energies in both its bound and free states. The relationship between ligand surrounding energies and free energy of binding is given by the equation

$$\Delta G_{\text{bind}} = \alpha\Delta\langle V_{\text{l–s}}^{\text{vdW}}\rangle + \beta\Delta\langle V_{\text{l–s}}^{\text{el}}\rangle$$

where $V_{\text{l–s}}^{\text{vdW}}$ and $V_{\text{l–s}}^{\text{el}}$ denote, respectively, the Lennard-Jones and electrostatic potentials between the ligand and its surroundings (l–s), which are evaluated as energy averages (denoted by $\langle\rangle$) from separate MD simulations of the free (solvated in water) and bound states. The difference (Δ) between such averages for each type of potential is scaled by different coefficients (see Ref. 37), giving the polar (electrostatic) and non-polar (van der Waals) contributions to the free energy. For the non-polar contribution, this coefficient has been empirically set to $\alpha = 0.181$, while for the polar contribution the scaling factor is dependent on the chemical nature of the ligand. For ligands with at least two hydroxyl groups, like the ones handled in this study, the value is $\beta = 0.33$.

Molecular dynamics were done using the program Q,[38] with the version of the OPLS all atom forcefield implemented there.[39] A 20 Å sphere of simulation was chosen, centered on the transition state mimic hydroxyl oxygen interacting with the catalytic aspartates. The sphere was solvated with TIP3P waters[40] with the water surface subjected to radial and polarization restraints[41] in order to mimic bulk water at the sphere boundary. Non-bonded interaction energies were measured up to a 10 Å cutoff, except for the ligand atoms where no cutoff was used. Beyond the cutoff, long-range electrostatics were treated with the local reaction field (LRF) multipole expansion method.[42] For the ligand–protein simulation, an equilibration phase was performed before the data collection phase. The equilibration protocol started with a 1000 step MD with very short time step (0.2 fs) at 1 K, coupled to a strong bath (0.2 fs bath coupling) thus similar to energy minimization. Then the system was gradually heated up to 300 K, relaxing the bath coupling to 10 fs and increasing the timestep to 1.5 fs. During this equilibration process, on Plm IV, hydrogen bonding constraints were imposed between the central hydroxyls and the aspartates (only one hydroxyl could be used for the 16-membered ring compounds). The need of these constraints is related to the non-optimal geometry that the 1LS5 structure shows for the catalytic aspartates. Unrestricted molecular dynamics followed then for 1.8–2.5 ns, making use of the SHAKE algorithm for the treatment of the bond lengths[43] and collecting energies at regular intervals of 15 fs. The MD was run until the energies collected showed stability for a period not shorter than 600 ps (collection period). Stability was addressed by comparing the average values of the first and second halves of the collection period.

The MD sampling of the free ligand was done using the same 20 Å water sphere of solvation. The solvent was equilibrated with a 10 ps MD at 300 K, in which the heavy atoms of the ligand were restrained through a 10 kcal/(mol Å^2) force constant. MD followed for more than 1.5 ns under the same conditions as for the bound state, but keeping the initial position of the central atom of the ligand fixed, to ensure a homogeneous solvation.

Acknowledgments

We thank the Swedish Foundation for Strategic Research (SSF/RAPID) and the Swedish Research Council (VR) for financial support.

References and notes

1. White, N. J. *J. Clin. Invest.* **2004**, *113*, 1084.
2. Breman, J. G. *Am. J. Trop. Med. Hyg.* **2001**, *64*, 1.
3. Wiesner, J.; Ortmann, R.; Jomaa, H.; Schlitzer, M. *Angew Chem., Int. Ed.* **2003**, *42*, 5274.
4. Coombs, G. H.; Goldberg, D. E.; Klemba, M.; Berry, C.; Kay, J.; Mottram, J. C. *Trends Parasitol.* **2001**, *17*, 532.
5. Francis, S. E.; Gluzman, I. Y.; Oksman, A.; Knickerbocker, A.; Mueller, R.; Bryant, M. L.; Sherman, D. R.; Russell, D. G.; Goldberg, D. E. *EMBO J.* **1994**, *13*, 306.
6. Boss, C.; Richard-Bildstein, S.; Weller, T.; Fischli, W.; Meyer, S.; Binkert, C. *Curr. Med. Chem.* **2003**, *10*, 883.
7. Banerjee, R.; Liu, J.; Beatty, W.; Pelosof, L.; Klemba, M.; Goldberg, D. E. *Proc. Natl. Acad. Sci. U.S.A.* **2002**, *99*, 990.
8. Berry, C. *Curr. Opin. Drug Dis. Dev.* **2000**, *3*, 624.
9. Omara-Opyene, A. L.; Moura, P. A.; Sulsona, C. R.; Bonilla, J. A.; Yowell, C. A.; Fujioka, H.; Fidock, D. A.; Dame, J. B. *J. Biol. Chem.* **2004**, *279*, 54088.
10. Liu, J.; Gluzman, I. Y.; Drew, M. E.; Goldberg, D. E. *J. Biol. Chem.* **2005**, *280*, 1432.
11. Ersmark, K.; Feierberg, I.; Bjelic, S.; Hulten, J.; Samuelsson, B.; Åqvist, J.; Hallberg, A. *Bioorg. Med. Chem.* **2003**, *11*, 3723.
12. Ersmark, K.; Feierberg, I.; Bjelic, S.; Hamelink, E.; Hackett, F.; Blackman, M. J.; Hulten, J.; Samuelsson, B.; Åqvist, J.; Hallberg, A. *J. Med. Chem.* **2004**, *47*, 110.
13. Ersmark, K.; Nervall, M.; Hamelink, E.; Janka, L. K.; Clemente, J. C.; Dunn, B. M.; Blackman, M. J.; Samuelsson, B.; Åqvist, J.; Hallberg, A. *J. Med. Chem.* **2005**, *48*, 6090.
14. Fairlie, D. P.; Tyndall, J. D. A.; Reid, R. C.; Wong, A. K.; Abbenante, G.; Scanlon, M. J.; March, D. R.; Bergman, D. A.; Chai, C. L. L.; Burkett, B. A. *J. Med. Chem.* **2000**, *43*, 1271.
15. Weber, A. E.; Halgren, T. A.; Doyle, J. J.; Lynch, R. J.; Siegl, P. K.; Parsons, W. H.; Greenlee, W. J.; Patchett, A. A. *J. Med. Chem.* **1991**, *34*, 2692.
16. Loughlin, W. A.; Tyndall, J. D. A.; Glenn, M. P.; Fairlie, D. P. *Chem. Rev.* **2004**, *104*, 6085.
17. Ghosh, A. K.; Devasamudram, T.; Hong, L.; DeZutter, C.; Xu, X.; Weerasena, V.; Koelsch, G.; Bilcer, G.; Tang, J. *Bioorg. Med. Chem. Lett.* **2005**, *15*, 15.
18. Tyndall, J. D. A.; Fairlie, D. P. *Curr. Med. Chem.* **2001**, *8*, 893.
19. Silva, A. M.; Lee, A. Y.; Gulnik, S. V.; Maier, P.; Collins, J.; Bhat, T. N.; Collins, P. J.; Cachau, R. E.; Luker, K. E.; Gluzman, I. Y.; Francis, S. E.; Oksman, A.; Goldberg, D. E.; Erickson, J. W. *Proc. Natl. Acad. Sci. U.S.A.* **1996**, *93*, 10034.
20. Tyndall, J. D. A.; Reid, R. C.; Tyssen, D. P.; Jardine, D. K.; Todd, B.; Passmore, M.; March, D. R.; Pattenden, L. K.; Bergman, D. A.; Alewood, D.; Hu, S.-H.; Alewood, P.

F.; Birch, C. J.; Martin, J. L.; Fairlie, D. P. *J. Med. Chem.* **2000**, *43*, 3495.
21. Li, T.; Yowell, C. A.; Beyer, B. B.; Hung, S.-H.; Westling, J.; Lam, M. T.; Dunn, B. M.; Dame, J. B. *Mol. Biochem. Parasitol.* **2004**, *135*, 101.
22. Oscarsson, K.; Lahmann, M.; Lindberg, J.; Kangasmetsa, J.; Unge, T.; Oscarson, S.; Hallberg, A.; Samuelsson, B. *Bioorg. Med. Chem.* **2003**, *11*, 1107.
23. Alterman, M.; Bjoersne, M.; Muehlman, A.; Classon, B.; Kvarnstroem, I.; Danielson, H.; Markgren, P.-O.; Nillroth, U.; Unge, T.; Hallberg, A.; Samuelsson, B. *J. Med. Chem.* **1998**, *41*, 3782.
24. Anon. *Synlett* **2003**, 423.
25. Åqvist, J.; Medina, C.; Samuelsson, J. E. *Protein Eng.* **1994**, *7*, 385.
26. Andrews, P. R. In *The Practice of Medicinal Chemistry*; Wermuth, C. G., Ed.; Academis Press: 1996; p. 345.
27. Yoshimura, N.; Tamura, M. Eur. Pat. Appl. 69339, 1983.
28. Westling, J.; Cipullo, P.; Hung, S.-H.; Saft, H.; Dame, J. B.; Dunn, B. M. *Protein Sci.* **1999**, *8*, 2001.
29. Dame, J. B.; Yowell, C. A.; Omara-Opyene, L.; Carlton, J. M.; Cooper, R. A.; Li, T. *Mol. Biochem. Parasitol.* **2003**, *130*, 1.
30. Haque, T. S.; Skillman, A. G.; Lee, C. E.; Habashita, H.; Gluzman, I. Y.; Ewing, T. J. A.; Goldberg, D. E.; Kuntz, I. D.; Ellman, J. A. *J. Med. Chem.* **1999**, *42*, 1428.
31. Copeland, R. A., Ed.; *Enzymes: A Practical Introduction to Structure, Mechanism, and Data Analysis* New York, 1996.
32. Cheng, Y.; Prusoff, W. H. *Biochem. Pharmacol.* **1973**, *22*, 3099.
33. ViewerPro 5.0, Accelrys Inc., San Diego, CA, 2002.
34. Westbrook, J.; Feng, Z. K.; Chen, L.; Yang, H. W.; Berman, H. M. *Nucleic Acids Res.* **2003**, *31*, 489.
35. Jones, G.; Willett, P.; Glen, R. C.; Leach, A. R.; Taylor, R. *J. Mol. Biol.* **1997**, *267*, 727.
36. Verdonk, M. L.; Cole, J. C.; Hartshorn, M. J.; Murray, C. W.; Taylor, R. D. *Prot. Struct. Funct. Genet.* **2003**, *52*, 609.
37. Hansson, T.; Marelius, J.; Åqvist, J. *J. Comput. Aided Mol. Des.* **1998**, *12*, 27.
38. Marelius, J.; Kolmodin, K.; Feierberg, I.; Åqvist, J. *J. Mol. Graph Modelling* **1999**, *16*, 213.
39. Jorgensen, W. L.; Maxwell, D. S.; TiradoRives, J. *J. Am. Chem. Soc.* **1996**, *118*, 11225.
40. Jorgensen, W.; Chandrasekhar, J.; Madura, J.; RW, I.; Klein, M. *J. Chem. Phys.* **1983**, *79*, 926.
41. King, G.; Warshel, A. *J. Chem. Phys.* **1989**, *91*, 3647.
42. Lee, F. S.; Warshel, A. *J. Chem. Phys.* **1992**, *97*, 3100.
43. Ryckaert, J. P.; Ciccotti, G.; Berendsen, H. J. C. *J. Compt. Phys.* **1977**, *23*, 327.